Influence of Ni−Co Catalyst Composition on Nitrogen Content in Carbon Nanotubes

A. G. Kudashov, A. V. Okotrub,* L. G. Bulusheva, I. P. Asanov,† Yu. V. Shubin, N. F. Yudanov, L. I. Yudanova, V. S. Danilovich, and O. G. Abrosimov‡

Nikolaev Institute of Inorganic Chemistry, SB RAS, pr. Ak. Lavrentieva 3, Novosibirsk 630090, Russia, Samsung Advanced Institute of Technology, P.O.Box 111, Suwon 440-600, Korea, and Boreskov Institute of Catalysis, SB RAS, pr. Ak. Lavrentieva 5, Novosibirsk 630090, Russia

Received: March 22, 2004; In Final Form: April 15, 2004

Nitrogen-containing carbon nanotubes were obtained by pyrolysis of acetonitrile (CH_3CN) at 850 °C over catalytic nanoparticles formed by the thermal decomposition of Co and Ni bimaleates or their mutual solutions. Structure and composition of synthesized samples were studied by electron microscopy, X-ray diffraction (XRD), and X-ray photoelectron spectroscopy (XPS). It is found that the yield of the nanotubes, the quality of the layer packing, and nitrogen content in the CN_x nanotubes depend on the catalyst composition. XPS of the N 1s spectra show that nitrogen atoms are in two different electronic states in the carbon nanotubes. According to quantum chemical calculations these states can be ascribed to nitrogen atoms substituting for carbon atoms in the graphite network and pyridine-like atoms. It was shown that the nanotubes synthesized using catalyst with the ratio Ni/Co 1:1 contain the greatest proportion of pyridine-like nitrogen.

Introduction

The substitution of nitrogen atoms for carbon in graphite layers of carbon nanotubes can result in the change of the electronic structure of the nanotubes and thus changes their physical properties. It was found that nitrogen atoms being electron donors improve the transport and field emission properties of the carbon nanotubes.[1,2] Theoretical predictions about superhardness of covalent compound C_3N_4 [3] also stimulated the development of synthesis techniques of nitrogen-containing tubes. Besides, the embedding of nitrogen atoms into a graphite framework can provide the selective reactivity of the carbon nanotubes.

Nitrogen-containing carbon nanotubes can be obtained by magnetron sputtering,[4] electric arc,[5] or laser evaporation of graphite[6] in a nitrogen atmosphere. The greatest quantity of nitrogen content (15−30%) was obtained using magnetron sputtering at 350 °C. The routine method for the synthesis of CN_x nanotubes is chemical vapor deposition (CVD) of nitrogen-containing compounds. This method is characterized by the simplicity of the experiment and allows for the variation of the parameters of the synthesis across a wide range and to obtain the material in large quantities. The catalysts of growth of the CN_x nanotubes are particles of 3d-transition metals—Ni, Co, and Fe formed in the decomposition of metal-organic compounds,[7−11] metallic films,[12] and metal powder coatings.[13] Ammonia or volatile nitrogen-containing organic compounds are generally used as a nitrogen source. The films of the ordered CN_x nanotubes vertically grown on different substrates were obtained by the pyrolysis of nickel phthalocianine[12,13] and the mixture of ferrocene and melamine.[11] The nitrogen concentration in the layers of the carbon nanotubes obtained by CVD is less than 15%.[1]

In this work, the influence of the Ni/Co ratio of the catalyst on the nanotube yield and nitrogen content was studied. The synthesis of catalyst is performed by one-stage decomposition of bimaleates of Ni and Co. Acetonitrile is used as a source of carbon and nitrogen. The obtained materials are examined by scanning electron microscopy (SEM), transmission electron microscopy (TEM), X-ray diffraction (XRD), and X-ray photoelectron spectroscopy (XPS).

Experimental Section

The catalysts were synthesized by the thermal decomposition of bimaleates of Ni and Co or their mutual solid solutions with the ratios of Ni/Co equal to 3:7, 1:1, and 7:3. These bimaleates are isostructural and form the continuous set of solid solutions. To synthesize the solid solutions the bimaleates were taken in their corresponding proportions, dissolved in water, and then dry evaporated at room temperature. According to an earlier study the thermolysis of these salts at 450 °C passes with the formation of composites containing metallic inclusions of size ∼5 nm in organic polymer.[14] It was suggested that at high temperature, ∼800 °C, polymer would form the carbon matrix preventing agglomeration of the individual nanoparticles.

The setup for a CVD synthesis of the carbon nanotubes was described in detail in ref 15. The CVD reactor is a stainless tube of length 1 m and diameter of 36 mm. Inside of the inner cavity a quartz tube of lesser diameter is placed. A low-gradient three-zone electric furnace with a firing zone size of ∼ 40 cm is put in the central part of the device. The setup is supplied with a temperature and gas flow control system. In the initial stage of the experiment a ceramic boat with pristine bimaleate powder was placed in the cold part of the device. The reactor was pumped out, filled with argon, and heated. The bimaleate powder was put into the zone heating to 850 °C. Acetonitrile vapor was fed into the reactor 10 min after the decomposition of bimaleate, with formation of metal nanoparticles. The synthesis time was 1 h. A grey-black substance was obtained

* To whom correspondence should be addressed. Tel: +7(3832) 305352. Fax: +7(3832) 344489. E-mail: spectrum@che.nsk.su.
† Samsung Advanced Institute of Technology.
‡ Boreskov Institute of Catalysis.

10.1021/jp048736w CCC: $27.50
Published on Web 05/27/2004

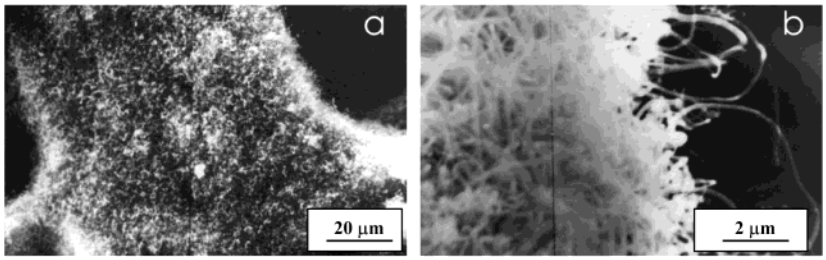

Figure 1. (a, b) SEM images of materials obtained using Ni/Co 1:1 catalyst and containing chaotically intertwined carbon nanotubes.

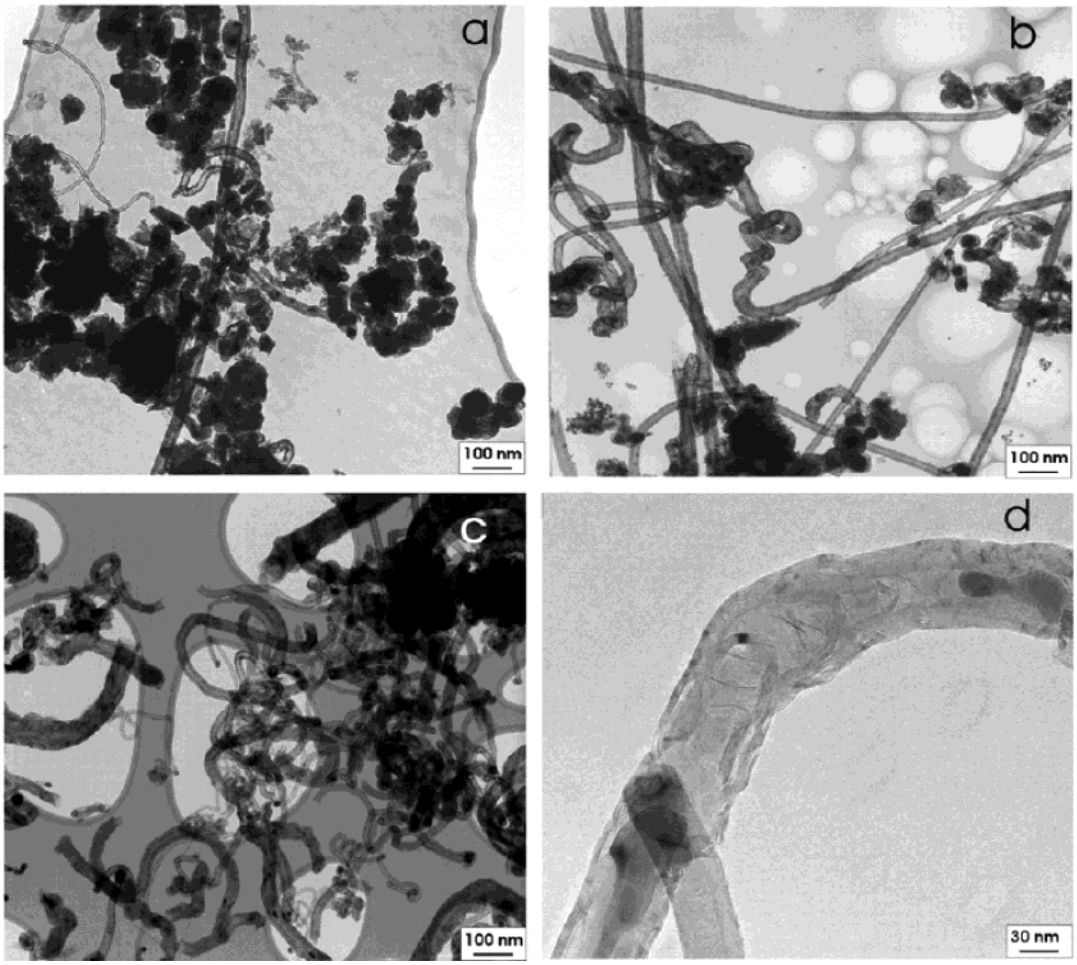

Figure 2. TEM images of materials obtained using as catalyst (a) Co, (b) Ni, and (c) Ni/Co 1:1. The magnified image of the CN_x nanotube (d) demonstrates the "loose" structure and low graphitization of the layers.

with volume exceeding that of the primary particles of salt crystals by 3−5 times. The granules of the obtained substance were disintegrated by weak mechanical action.

The synthesized samples were studied with a scanning electron microscope JEOL ET-200, a transmission electron microscope JEOL-100C, an XPS spectrometer Quantum 2000 Scanning ESCA Microprobe, and an X-ray diffractometer DRON-SEIFERT-RM4.

Results

SEM and TEM Results. The typical SEM image of the synthesized material is shown in Figure 1a and b. The granules of size 30−100 μm are a ball of intertwined carbon nanotubes. TEM images of the samples obtained using Co, Ni, and Ni/Co 1:1 catalysts are presented in Figure 2. The synthesized materials contain carbon nanotubes, catalyst particles capsulated into graphite shells, and amorphous carbon. The tubes are multi-walled with almost invariable thickness. As can be seen, the content of the carbon nanotubes in the sample and their structure are substantially determined by the catalyst type. The material synthesized using Co bimaleate is the most contaminated by amorphous carbon particles (Figure 2a). These particles are fragments of the carbon matrix that are not destroyed at the temperature in the CVD reactor. Analysis of the TEM images of the sample showed that the diameter and the thickness of walls of the nanotubes vary in the interval 30−40 and 12−15 nm, correspondingly. For the nanotubes obtained on Ni catalysts the respective diameter and thickness vary within 20−40 and 12−15 nm (Figure 2b). The sample obtained using Ni/Co 1:1 catalyst contains tubular structures of diameter 60−90 nm with a wall thickness of 20−35 nm and thinner nanotubes 15−30 nm in diameter and 5−7 nm in wall thickness (Figure 2c). The nanotubes obtained from this catalyst are characterized by embedding of metal nanoparticles into inner cavities and the walls of the tubes. The separation of the metal clusters from the liquid catalytic particle takes place in the process of growth

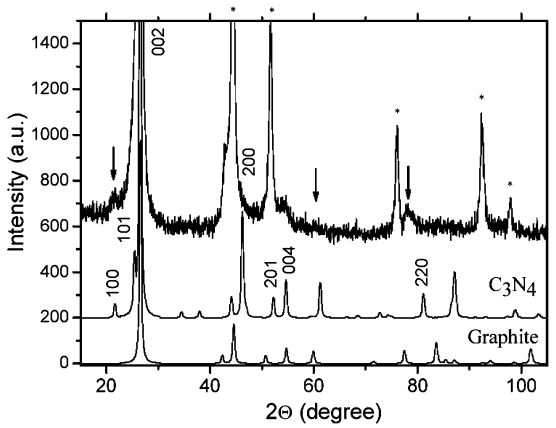

Figure 3. Diffractogram of the sample obtained with Ni/Co 3:7 catalyst. The bottom panels show difractograms of hexagonal C_3N_4 and graphite. The reflections from fcc of the metal catalyst are marked by asterisks (∗), and the reflections from C_3N_4 planes and graphite are indexed.

TABLE 1: X-ray Diffraction Data for Samples Synthesized Using Different Catalysts

catalyst composition	lattice parameter of catalyst (Å)	av size of catalyst (nm)	fwhm of the (002) reflection of carbon nanotube (grad)
Co	3.544(3)	12	1.65
Ni/Co 3:7	3.539(3)	20	1.85
Ni/Co 1:1	3.534(3)	25	1.40
Ni/Co 7:3	3.529(3)	22	1.55
Ni	3.525(3)	30	2.05

of the nanotubes that can be attributed to the features of the Ni/Co particle, for example, the lower values of the surface tension coefficient and the melting temperature. The maximum content of the nanotubes is observed in the sample obtained using Ni/Co 1:1 catalyst.

The carbon nanotubes synthesized in the present work are characterized by the "loose" structure of the layers. The magnified TEM image of the nanotube demonstrates the high defectiveness of the walls of the tube with conical layer packing (Figure 2d). The layers do not form the bridges perpendicular to the tube axis, and the inner channel is open. TEM study of the synthesized samples showed that the CN_x nanotubes are formed only on rather large metal particles of size 15 nm and greater. The smaller particles formed in the process of the bimaleate decomposition do not participate in the nanotube growth.

X-ray Diffraction. The XRD profiles of the samples obtained using different catalysts are characterized by the same set of the reflections. As the example the difractogram of the powder material synthesized on the Ni/Co 3:7 catalysts is shown in Figure 3. The sharp peaks at the angles $2\theta = 44.5°$, 51 °, 77 °, 92 °, and 98° (marked by *) correspond to the (111), (200), (220), (311), and (420) reflections of the face-centered cubic lattice (fcc) of metal particles occurred in sample. The refined values of the lattice parameter $\boldsymbol{a}$ are presented in Table 1. For Ni and Co catalysts the parameter $\boldsymbol{a}$ equals to that of the bulk samples. It is worth noting that fcc of Co is metastable and can be obtained only at fast high-temperature hardening of metal. The value of the lattice parameter for bimetallic catalysts is changed additively with the variation of the ratio of metals in according to Vegard's rule. This fact points to the formation of the solid solutions from the mixture of Ni and Co. The average sizes of the coherent scattering areas vary from 12 to 30 nm as derived from the integral broadening of the diffraction peaks.

TABLE 2: Parameters of the N 1s Spectra of Samples Synthesized Using Different Catalysts

catalyst composition	nitrogen content (%)	binding energy peak A (eV)	binding energy peak B (eV)	rel intensity of peaks A/B
Co	0.70	398.74	401.78	0.47
Ni/Co 3:7	0.50	399.11	401.79	0.83
Ni/Co 1:1	1.20	399.19	401.79	1.28
Ni/Co 7:3	0.60	399.29	401.88	0.55
Ni	1.20	398.99	401.66	0.34

These values agree well with the metal particle sizes determined from the TEM images.

The other reflections are described by diffraction from the graphite-like lattice of the carbon nanotubes and on the whole correspond to the difractogram of hexagonal graphite shown in Figure 3 for comparison. In addition, the XRD pattern exhibits weak reflections that cannot be ascribed to the graphite lattice. These reflections could be indexed analogously to the hexagonal C_3N_4 (Figure 3) belonging to sp.gr.-6m2 (ICSD-83265). The parameters derived from the XRD pattern of nanotubes are equal to $\boldsymbol{a} = 4.86(1)$ Å and $\boldsymbol{c} = 6.75(1)$ Å, which is markedly different from graphite and carbonitride lattice parameters. Unfortunately, it is impossible to determine the lattice parameters with high accuracy because of the significant broadening of the reflections and overlapping some of them with the metal phase reflections. The tabular values for graphite are $2 \times \boldsymbol{a} = 4.928$ Å, $\boldsymbol{c} = 6.711$ Å, for C_3N_4 $\boldsymbol{a} = 4.742$ Å, $\boldsymbol{c} = 6.721$ Å. The parameter $\boldsymbol{a}$ is defined by hexagons composing the layers of the CN_x nanotubes and lies between the values for carbonitride and twice value $\boldsymbol{a}$ for hexagonal graphite. The observed diffraction pattern points to quite homogeneous distribution of nitrogen atoms in the nanotube walls. However, the question of the order in the arrangement of nitrogen is open. The parameter $\boldsymbol{c}$ in the nanotubes exceeds the corresponding value for graphite and carbonitride. The change of the diffraction angles in the samples under study indicates that the carbon nanotubes obtained using Ni/Co 1:1 catalyst have the least interlayer spacing d_{001}. The least broadening (fwhm) of the (002) reflection of carbon nanotubes grown from the Ni/Co 1:1 solid solution (Table 1) indicates the most quality packing of the graphite layers. The maximum of layer disordering is characteristic of the nanotubes synthesized using Ni and Ni/Co 3:7 catalyst particles.

XPS Data. The concentration of nitrogen in the samples was estimated from the ratio of the areas of the N 1s and C 1s lines with taking into account the photoionization cross-sections. The dependence of nitrogen content on the catalyst composition is presented in Table 2. The samples obtained on Ni and Ni/Co 1:1 catalysts involve the maximum of nitrogen (∼1.2%). Acetonitrile, used as a source for CN_x nanotube formation, contains ca. 34 wt % nitrogen, and the low ratio of nitrogen in the products could be attributed to the formation of HCN in the gas phase at elevated temperature.[16] The nitrogen concentration in the samples is more likely determined by the nature of metallic nanoparticles, which catalyze the formation of carbon nanotubes.[17,18] It is generally accepted that hydrocarbon first decomposes at the surface of the catalyst and then carbon atoms diffuse to the bulk and precipitate at the other side of the catalytic particle, initiating growth of a graphitic layer.[19] It has been shown that the nitrogen is also incorporated in the catalyst surface and its concentration in the tube shells increases with increasing growth rate of carbon nanotubes.[12] Among transition metals nickel provides the highest rate of multiwall nanotube growth,[20] which could be responsible for the maximum amount of nitrogen in the sample obtained on Ni catalyst. The high degree of nitrogen doping found for the CN_x tubes grown from

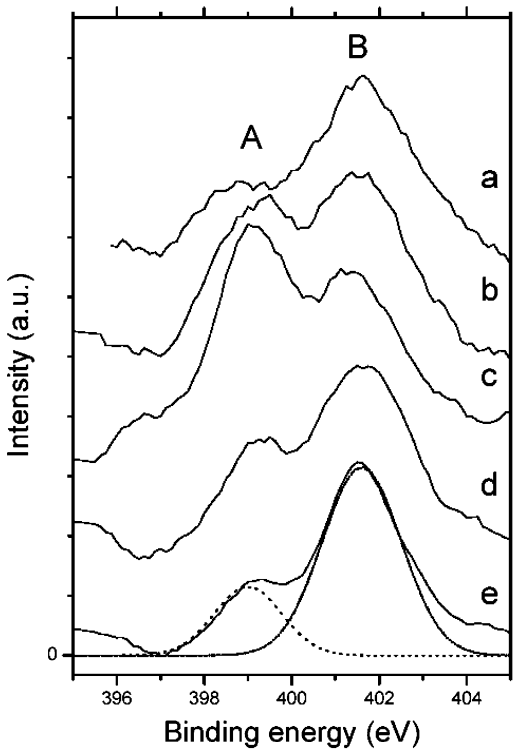

Figure 4. N 1s spectra of the sample obtained using as catalyst (a) Co, (b) Ni/Co 3:7, (c) Ni/Co 1:1, (d) Ni/Co 7:3, and (e) Ni. The spectrum of sample (e) is fitted with two Gaussian components.

the Ni/Co 1:1 catalyst may be connected with the change of the solubility of nitrogen in the metal particles. Indeed, nitrogen shows the greatest solubility in the Ni/Co 1:1 solid solution.[21]

The general peculiarity of the N 1s spectra is the presence of two peaks A and B at 399 and 401.6 eV, respectively (Figure 4). The splitting of the N 1s line indicates that the nitrogen atoms are in at least two different chemical states in the synthesized samples. For the estimation of the relative content of the different nitrogen atoms the spectra were fitted by two Gaussian components of the width 2.1 eV. The example of the fitting is demonstrated for the sample obtained using Co catalyst. The change of the relative intensity of the peaks A/B in the samples under study is presented in Table 2. The maximal relative intensity of the peak A is achieved for the sample synthesized using Ni/Co 1:1 catalyst.

Quantum Chemical Simulation of the N 1s Spectra. The inserting of nitrogen in the graphite network results in the splitting of the N 1s line that is observed in the XPS spectra of CN_x nanotubes[1,6,12] and CN_x films.[22−24] The interpretation of the splitting is ambiguous. The higher binding energy peak in the N 1s spectra is usually related to the nitrogen atoms substituting for carbon in the graphite layer and bound with three sp^2-hybridized carbon atoms. The peak A around 399 eV can correspond to different nitrogen atoms. So this maximum may be related to nitrogen attached to carbon in sp^3-hybridization[12,22,23] or forming NH_2 groups on the edges of the graphite layers of CN_x tubes.[8] The simulation of the tunneling microscopy data for the CN_x nanotubes suggests the presence of nitrogen atoms having two bonds with neighboring carbon atoms in the walls of the tubes, that is, the so-called pyridine-like nitrogen,[1] which may be responsible for the formation of the lower binding energy peak in the N 1s spectrum. For the interpretation of the N 1s spectrum of amorphous CN_x films ab initio 6-31*G calculations of the core levels of the different nitrogen-containing molecules and clusters were performed.[22] The

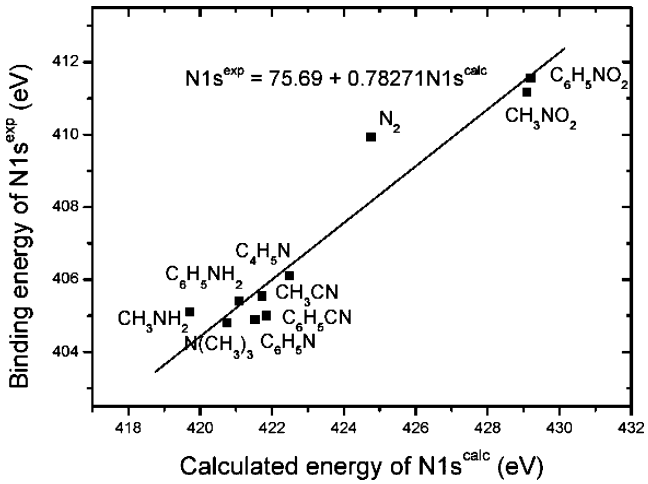

Figure 5. Dependence of the measured binding energies of the N 1s level (vertical axis) on calculated binding energies in the Hartee−Fock approximation (horizontal axis) for 10 test nitrogen-containing molecules. The expression on the top of the figure describes the linear function.

estimation of the chemical shift of the N 1s level was determined in terms of Coopmans' theorem. The obtained values were corrected to take into account the electron relaxation accompanying the photoionization process. The correction factor was determined from the comparison between the experimental and theoretical values corresponding to the difference of the binding energies of the inner levels of nitrogen and carbon in the molecules of pyridine and pyrrol.[25] Taking into account the theoretical values of the binding energies, the higher and lower binding energy peaks in the N 1s spectra of the CN_x films were ascribed to the nitrogen atoms bonded to the carbon atoms in sp^2- and sp^3-hybridized states, correspondingly.

In the present work we use the similar approach for interpretation of the N 1s spectra of the CN_x nanotubes. The correction factor was determined from the correlation dependence between the experimental and theoretical values for 10 nitrogen-containing molecules: N_2, CH_3CN, CH_3NH_2, CH_3NO_2, $N(CH_3)_3$, C_5H_5N, C_4H_5N, $C_6H_5NH_2$, $C_6H_5NO_2$, and C_6H_5CN. The energy of the N 1s level was calculated by the Hartree−Fock approximation with 3-21G basis set using the quantum chemical package Jaguar.[26] The obtained data were compared with the experimental binding energies,[27] and the linear correlation dependence was built for taking into account the relaxation effects beyond of the calculation (Figure 5). The experimental values of the control compounds lie fairly within the linear dependence except for that of the nitrogen molecule. Correlation factor between the experimental and predicted approximation line is 0.96.

The study of the influence of the sp^2-carbon surrounding on the N 1s binding energy was performed according to the results of the calculation for the four model structures, with two of them shown in Figure 6. Model **1** is the graphite cluster with the nitrogen atom substituting for central atom. A result of the attachment of hydrogen atoms to the boundary cluster atoms is that the composition of the model **1** corresponds to $C_{36}NH_{15}$. The embedding of the pyridine-like nitrogen into the graphite framework is possible only if the atomic vacancy exists.[28] Model **2** contains three pyridine-like nitrogen atoms and has the composition $C_{33}N_3H_{15}$. Models **3** and **4** are obtained from model **2** by replacing correspondingly one or two pyridine-like nitrogen atoms with carbon atoms. The structure of the models was optimized within the framework of the aforementioned quantum chemical approach. The calculated values of the N 1s energy

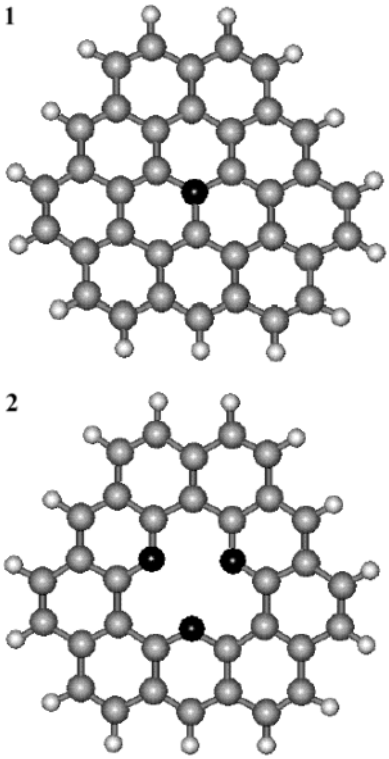

Figure 6. Optimized structures of model **1** (nitrogen substitutes for carbon atom in graphite cluster) and model **2** (graphite cluster contains three pyridine-like nitrogen atoms). Hydrogen atoms are connected to the boundary carbon atoms.

levels were corrected in accordance with the dependence on Figure 5 and the work function of the spectrometer (6 eV). The obtained value of the binding energy of the N 1s level in model **1** is 401.68 eV, which is practically equal to the position of peak B in the spectra of the samples under study (Table 2).

Binding energies determined according to calculation of the models **2**, **3**, and **4** are equal to 399.04, 400.12, and 400.62 eV, correspondingly. The structure with three pyridine-like atoms surrounding a vacancy in the graphite network (model **2**) gives the best fit to peak A in the N 1s spectra of the samples under study. Position and width of peak A are somewhat changed with the variation of the catalyst composition (Figure 4 and Table 2). We may propose that the carbon nanotubes obtained from the mixed Ni/Co catalysts contain some quantity of nitrogen atoms with chemical state corresponding to models **3** and **4**. Just the spectra of these samples show the shift of the peak A to the higher binding energies. It is worth noting that the N 1s binding energy calculated for NH_2 groups corresponds well to the peak A. However, it is difficult to expect the formation of a great deal of such groups at the high temperatures of the synthesis condition.

Conclusion

CN_x nanotubes were synthesized by CVD technique by decomposition of acetonitrile at 850 °C using Ni/Co catalysts. The particles with different ratios of Ni and Co are formed as a result of thermolysis of bimaleates of Co and Ni and their solid solutions. The maximum yield of the CN_x nanotubes, the best packing of layers, and the greatest concentration of nitrogen were found for the material obtained using the Ni/Co 1:1 catalyst. The crystallinity of carbon nanotubes is mainly determined by composition and morphology of catalytic particles, and in our synthetic conditions the Ni/Co 1:1 solid solution has more uniform catalytic activity. X-ray diffraction studies suggest the homogeneous distribution of nitrogen in the layers of the CN_x nanotubes. The embedding of nitrogen into the graphite shells leads to the appearance of the reflections close to those in hexagonal C_3N_4 where nitrogen is two-coordinated (pyridine-like). According to XPS data the nitrogen content is maximal (~1.2%) for the samples obtained using the Ni and Ni/Co 1:1 catalysts. The splitting of the N 1s line is changed with the variation of catalyst composition and points to the realization of the different chemical states of nitrogen in the samples. Ab initio calculations of the binding energies of the inner levels in the different nitrogen-containing molecules and graphite clusters are used for interpretation of the N 1s spectra. It was shown that the higher and lower binding energy peaks are connected with the three- and two-coordinated nitrogen atoms, correspondingly. The greatest proportion of the pyridine-like nitrogen was found for the sample obtained with the Ni/Co 1:1 catalyst. The equal quantity of Ni and Co in the catalyst provides the higher solubility of nitrogen in the metal particle and probably higher kinetics of growth of the CN_x nanotube. It results in formation of the high number of vacancies in the nanotube walls with nitrogen atoms on the boundaries.

Acknowledgment. The work was financially supported by RFBR (grants 03-03-32286, 03-03-32336) and a grant from the President of Russian Federation for support of scientific schools no. NS-1042.2003.3. A.G.K. acknowledges HALDOR TOPSOE Company for financial support.

References and Notes

(1) Terrones, M.; Ajayan, P. M.; Banhart, F.; Blasé, X.; Carroll, D. L.; Charlier, J. C.; Czerw, R.; Foley, B.; Grobert, N.; Kamalakaran, R.; Kohler-Redlich, P.; Ruhle, M.; Seeger, T.; Terrones, H. *Appl. Phys. A* **2002**, *74*, 355.

(2) Golberg, D.; Dorozhkin, P. S.; Bando, Y.; Dong, Z.-C.; Tang, C. C.; Uemura, Y.; Grobert, N.; Reyes-Reyes, M.; Terrones, H.; Terrones, M. *Appl. Phys. A* **2003**, *76*, 499.

(3) Liu, A. Y.; Cohen, M. L. *Science* **1989**, *245*, 841.

(4) Suenaga, K.; Johanson, M. P.; Hellgren, N.; Broitman, E.; Wallenberg, L. R.; Colliex, C.; Sungren, J. E.; Hultman, L. *Chem. Phys. Lett.* **1999**, *300*, 695.

(5) Zhang, Y.; Gu, H.; Suenaga, K.; Iijima, S. *Chem. Phys. Lett.* **1997**, *279*, 264.

(6) Droppa, R., Jr.; Hammer, P.; Carvalho, A. C. M.; dos Santos, M. C.; Alvarez, F. *J. Non-Cryst. Solids* **2002**, *299*−*302*, 874.

(7) Yudasaka, M.; Kikuchi, R.; Ohki, Y.; Yoshimura, S. *Carbon* **1997**, *35*, 195.

(8) Suenaga, K.; Ydasaka, M.; Colliex, C.; Iijima, S. *Chem. Phys. Lett.* **2000**, *316*, 365.

(9) Han, W.-Q.; Kohler-Redlich, P.; Seeger, T.; Ernst, F.; Ruhle, M.; Grobert, N.; Hsu, W.-K.; Chang, B.-H.; Zhu, Y.-Q.; Kroto, H. W.; Terrones, M.; Terrones, H. *Appl. Phys. Lett.* **2000**, *77*, 1807.

(10) Lee, C. J.; Lyu, S. C.; Kim, H.-W.; Lee, J. H.; Cho, K. I. *Chem. Phys. Lett.* **2002**, *359*, 115.

(11) Terrones, M.; Terrones, H.; Grobert, N.; Hsu, W. K.; Zhu, Y. Q.; Kroto, H. W.; Walton, D. R. M.; Kohler-Redlich, Ph.; Ruhle, M.; Zhang, J. P.; Cheetham, A. K. *Appl. Phys. Lett.* **1999**, *75*, 3932.

(12) Kim, T.-Y.; Lee, K.-R.; Eun, K. Y.; Oh, K.-H. *Chem. Phys. Lett.* **2003**, *372*, 603.

(13) Sen, R.; Satishkumar, B. C.; Govindaraj, A.; Harikumar, K. R.; Raina, G.; Zhang, J. P.; Cheethan, A. K.; Rao, C. N. R. *Chem. Phys. Lett.* **1998**, *287*, 671.

(14) Logvinenko, V. A.; Yudanov, N. F.; Chekhova, G. N.; Kriger, Yu. G.; Yudanova, L. I.; Rudina, N. A. *Chem. Sustainable Dev.* **2000**, *8*, 171.

(15) Kudashov, A. G.; Okotrub, A. V.; Yudanov, N. F.; Romanenko, A. I.; Bulusheva, L. G.; Abrosimov, O. G.; Chuvilin, A. L.; Pazhetnov, E. M.; Boronin, A. I. *Phys. Solid State* **2002**, *44*, 626.

(16) Hao, Y.; Qingwen, L.; Jin, Z.; Zhongfan, L. *Chem. Phys. Lett.* **2003**, *380*, 347.

(17) Iijima, S.; Ichihashi, T. *Nature* **1993**, *363*, 603.

(18) Bethune, D. S.; Kiang, C. H.; de Vries, M. S.; Gorman, G.; Savoy, R.; Vazquez, J.; Beyers, R. *Nature* **1993**, *363*, 605.

(19) Jourdain, V.; Kanzow, H.; Castignolles, M.; Loiseau, A.; Bernier, P. *Chem. Phys. Lett.* **2002**, *364*, 27.

(20) Huang, Z. P.; Wang, D. Z.; Wen, J. G.; Sennett, M.; Gibson, M.; Ren, Z. F. *Appl. Phys. A* **2002**, *74*, 387.
(21) Kowanda, C.; Speidel, M. O. *Scr. Mater.* **2003**, *48*, 1073.
(22) Souto, S.; Pickholz, M.; dos Santos, M. C.; Alvarez, F. *Phys. Rev. B* **1998**, *57*, 2536.
(23) Hellgren, N.; Johanson, M. P.; Broitman, E.; Hultman, L.; Sundgren, J.-E. *Phys. Rev. B* **1999**, *59*, 5162.
(24) Ohta, R.; Lee, K. H.; Saito, N.; Inoue, Y.; Sugimura, H.; Takai, O. *Thin Solid Films* **2003**, *434*, 296.
(25) Casanovas, J.; Ricart, J. M.; Rubio, J.; Illas, F.; Jimenez-Mateos, J. M. *J. Am. Chem. Soc.* **1996**, *118*, 8071.
(26) *Jaguar 3.5*; Schrodinger, Inc.: Portland, OR, 1998.
(27) Bakke, A. A.; Chen, H.-W.; Jolly, W. L. *J. Electron. Spectrosc. Relat. Phenom.* **1980**, *20*, 333.
(28) Miyamoto, Y.; Cohen, M. L.; Louie, S. G. *Solid State Commun.* **1997**, *102*, 605.